High-frequency FWI Imaging: repurposing seismic data for imaging shallow hazards

Hung Dinh[1]*, Thomas Latter[1], Mike Townsend[2], Nils Grinde[2], Ståle Høgden[2], Nicholas Robb[2], Marte Aksland[2] and Alexander Bertrand[2] demonstrate that high-frequency FWI and associated attributes can help to identify shallow anomalies and fault systems more effectively than standard imaging methods, with a significant increase in resolution.

Abstract

Dedicated high-resolution site surveys are used to identify potential hazards prior to the placement of infrastructure. Apart from the additional acquisition expense, site surveys are often acquired as a series of 2D lines, which limits their spatial resolution. We describe how FWI Imaging results from existing, raw, conventional 3D seismic data, can be used as a rapidly available 3D alternative or supplementary dataset to help improve understanding of the shallow subsurface. Two case studies demonstrate the potential of this approach. Specifically, they show that high-frequency FWI and associated attributes can help to identify shallow anomalies and fault systems more effectively than standard imaging methods, with a significant increase in resolution. Furthermore, FWI has proven its ability to provide shallow image quality comparable to that of multibeam echo sounder measurements, even with less densely acquired data.

Introduction

Understanding shallow geohazards is a critical consideration due to their potential impact on infrastructure placement. In oil and gas applications, challenges ranging from gas seepages, shallow water flow, or unstable soil conditions pose risks to drilling operations. However, achieving the necessary resolution in the near surface can present a challenge even to 3D seismic data, which has been acquired specifically for shallow imaging. Conventional 3D towed-streamer data for exploration purposes (referred to here as 'conventional 3D' data), acquired for deeper (>500 m) targets, is more readily available. Conventional 3D acquisition geometries (narrow azimuth, multiple streamers) imaged with traditional processing flows (applying standard migration algorithms imaging only primary reflections) are unlikely to provide sufficient resolution for shallow hazard analysis. This is the result of poor crossline sampling and limited near-offset coverage with large azimuthal variations.

A longstanding solution for shallow hazard imaging has been the acquisition of 2D high-resolution (2DHR) site surveys (Douglas, 2011). These employ specialised acquisition equipment, yielding high sampling rates along the survey line. However, 2DHR site surveys usually lack the necessary spatial resolution between the survey lines (typically spaced 150-300 m apart) and incorrectly image features with a degree of geometric heterogeneity owing to erroneous imaging of reflection points outside the 2D plane. Geological details can therefore be missed that would help operators distinguish between sites for safe infrastructure placement from those harbouring unforeseen hazards. Dedicated 3D high-resolution (3DHR) site surveys can overcome these limitations (Kassarie et al., 2017), but these come with substantially higher financial investment, limiting their widespread application.

In some cases, a hybrid approach has been adopted, which combines a 2DHR site survey with a conventionally imaged 3D seismic survey. This approach aims to combine the advantages of the high temporal resolution of the 2DHR survey with the 3D imaging benefits of a conventional 3D survey. However, case studies using this approach result in a conventional 3D survey suffering from suboptimal resolution, as well as delivering an inconsistent interpretation with 2DHR site surveys. This leaves a gap between localised high-resolution information and the broader regional context (Sharp and Samuel, 2004; Selvage et al., 2012).

Alternatives without new data acquisition

Reprocessing of conventional 3D towed-streamer data with workflows to recover more near-surface resolution is not new (Kanrar et al., 2019). However, the traditional Kirchhoff algorithms utilised are limited by technical constraints, such as ray tracing and velocity approximations, sampling constraints including the near-offset sampling gap, or illumination imbalances. These constraints chiefly originate from the use of only primary reflection energy. Two recent alternatives are the use of near-field hydrophone (NFH) data, which is readily available for routine monitoring of the source and designing the source signature, and multiple imaging techniques. NFH data may provide high-resolution imaging results owing to their dense sub-millisecond sampling (Tyagi et al., 2021). Meanwhile, multiple migration improves image quality by using recorded data as secondary sources (Poole, 2021). These two methods have been compared by various authors as approaches to enhance shallow imaging

(Lim et al., 2022; Tang et al., 2023). However, some pitfalls of NFH imaging lie in the low-fold nature of the data, difficulty in removing the direct arrival, the requirement for a full processing flow, and the challenge of addressing the sampling gap between source lines. Multiple imaging, on the other hand, is sometimes limited by its Born-approximated wave-equation that does not always perform accurately in complex shallow intervals (Lu, 2021).

Given the limitations above, Full-waveform inversion (FWI) offers an alternative approach utilising a two-way wave equation. Leveraging the full wavefield, including multiples, ghost energy and diving waves, from raw seismic data results in unparalleled subsurface sampling and illumination. FWI can deliver accurate models and quantitative estimates of subsurface properties rapidly through an iterative inversion process. Although significant computational power is required, advances in algorithms and high-performance computing have accelerated rollout. For example, Time-lag FWI (TLFWI; Zhang et al., 2018; Wei et al., 2023) has facilitated high-resolution models at more than 100 Hz. Having the potential to naturally compensate for illumination and transmission loss (Cooper and Ratcliffe, 2023), FWI can provide more accurate subsurface information and has become essential for imaging complex structures where conventional approaches struggle (Zhang et al., 2020). This helps compensate for the imaging limitations of 2DHR surveys and conventional 3D towed-streamer imaging, especially in the near surface.

Previous FWI work on shallow hazards
As early as ten years ago, FWI was applied to invert for shallow overburden velocities up to 9 Hz using reflections, diving waves, and refracted head waves (Wiarda et al., 2014). Small-scale gas bodies were identified and correlated to 2DHR site survey data for the first time by Bright et al. (2015) in a 7 Hz FWI anomaly

Figure 1 Basemap showing two case study areas in the Northern Viking Graben area, and the Barents Sea.

volume, which was built using narrow-azimuth towed-streamer data. Reaching mid-teen frequencies, while using conventional wide-azimuth towed-streamer data, Li et al. (2015) showed that FWI can detect gas bodies more confidently and effectively than conventional tomography. However, the resolution of the anomalies from these studies was still subpar compared to standard 2DHR data. Recently, FWI technology has advanced in assessing shallow hazards. With sparse OBC acquisition, a 20 Hz FWI study demonstrated superior resolution on shallow gas pockets, outperforming a 25 Hz RTM image despite acquisition sparsity (Vandrasi et al., 2020).

The most recent FWI studies by Latter et al. (2022), Espin et al. (2023) and Dinh et al. (2023, 2024) demonstrate such applications by pushing the inversion maximum frequency limit, in some cases above 100 Hz. Here, we investigate the feasibility of FWI for shallow hazard analysis, aided by attribute analysis on the FWI velocities and their associated derivatives from two recent studies (Figure 1). Examples include bathymetry maps, attribute extractions for low-velocity anomalies, and fault systems, which are then compared against 2DHR and conventionally imaged towed-streamer datasets.

Methodology
Seismic attribute analyses have often been used to assess geological properties, as they can reveal hidden responses from hazard features in regular amplitude sections (Sukmono et al., 2017; Tokarev et al., 2018).

For shallow hazards, attribute analysis can be performed directly on the FWI impedance model, I_p, or from the FWI Image derived as its spatial derivative:

$$FWI_{Image} = \frac{\partial I_p}{\partial x}\sin\theta\cos\varphi + \frac{\partial I_p}{\partial y}\sin\theta\sin\varphi + \frac{\partial I_p}{\partial z}\cos\theta , \qquad (1)$$

given dip θ and azimuth φ of the normal vector n to the subsurface reflector (Zhang et al., 2020). Here, for simplicity, we consider the velocity-only version of this derivative.

Shallow geohazard attributes
Most common subsurface hazards have distinct velocity contrasts from their surroundings. Based on Bright et al. (2015), we propose a stable and accurate velocity anomaly extraction A by subtracting the median background velocity $\hat{v}$ from the high-resolution FWI model v:

$$A = v - \hat{v} . \qquad (2)$$

The use of the median can help to detect small-scale anomalies more effectively, whereas using the mean or smoothing can suffer from anomaly outliers. This approach can detect a wide variety of overburden shallow anomalies, likely associated with gas pockets, shallow water-flow sands, boulders, pressure zones and pipelines.

Bathymetry map extraction
To detect the seabed or seabed features, a surface can be extracted based on the distinct velocity differences between sediment and seawater. Alternatively, this can be estimated by the depth at which the maximum derivative of the FWI Image is found:

$$Z_{wb_{x,y}} = argmax\left(\partial FWI_{Image}\right). \tag{3}$$

This is expected to identify the water bottom as the strongest contrast between the water layer and sediment. However, with an unconsolidated seabed including mixed layers of soft and hard clay, the maximum derivative may represent the boundary between clay layers. To help minimise this, prior information about the water column, such as temperature salinity data, can be useful.

From the bathymetry map, two attributes can be calculated:
- The seabed surface gradient can reveal natural hazards, such as pockmarks, iceberg scours, unstable slopes, sink holes, or surface channels, present between two points A and B with their X and Y positions respectively, and water bottom depth Z as follows:

$$WBdip_{AB} = arctan\left(\frac{Z_A - Z_B}{\sqrt{\left(X_A - X_B\right)^2 + \left(Y_A - Y_B\right)^2}}\right). \tag{4}$$

- An amplitude map extracted from the FWI velocity within a small interval below the seabed surface can reveal man-made seabed features such as cables, shipwrecks and debris from previous exploration or production operations.

Fault detection
Standard spatial coherency is an effective attribute to detect faults (Sukmono et al., 2017). A modified dip-coherency was introduced to aid interpretation by taking the root-mean-square (RMS) of the spatial derivatives of the velocity with respect to the plane of the reflector along and perpendicular to the local azimuth direction, n_{Az} and n_{Az+90}, respectively, as described by Kerrison et al. (2021):

$$RMS = \sqrt{\left(\frac{\partial v}{\partial n_{Az}}\right)^2 + \left(\frac{\partial v}{\partial n_{Az+90}}\right)^2}. \tag{5}$$

A similar approach can be extended to the FWI Image (following Equation 1) to highlight different features in the FWI results.

Example 1
Data description
The Dugong area, located in the Northern Viking Graben area with a 330 m water depth, was surveyed by two 3D towed-streamer narrow-azimuth acquisitions: a 2016 north-south oriented variable-depth towed-streamer dataset and a 2020-2021 east-west multi-sensor dataset. Both deployed 8 km streamers with a 75 m separation and were processed using advanced Q-honouring dual-azimuth (DAZ) processing and multi-parameter velocity model building flow (Latter et al., 2022).

A 2020 2D high-resolution site survey with line spacing of 100 m provided bathymetric, seabed and sub-seabed data, focusing on shallow gas hazards within an interval at a 430-465 m depth (550-590 ms TWT). The 2DHR site survey included multibeam echo sounder (MBES) data, from which a three-cell smoothed 3 m × 3 m bathymetry map was created. The 2DHR site survey also featured high-resolution 96-channel seismic acquisition at a sample rate of 1 ms with a 12.5 m channel interval, resulting in a 2D CMP spacing of 6.25 m. From this, a shallow gas hazard map was generated in the gas warning interval by combining amplitude anomalies from the 2DHR seismic lines and extrapolating their spatial extent using amplitudes picked from the existing 2016 north-south 3D seismic data (Figure 4a). This approach aimed to improve spatial accuracy and delineate shallow gas hazards that may have been missed by the 2DHR data.

A 40 km² area covering the 2DHR survey was selected for this DAZ case study. The raw 3D DAZ seismic data was utilised to generate a high-resolution 100 Hz visco-acoustic TLFWI Image. Subsequently, bathymetry and gas hazard maps were calculated from the FWI Image and velocity model, respectively.
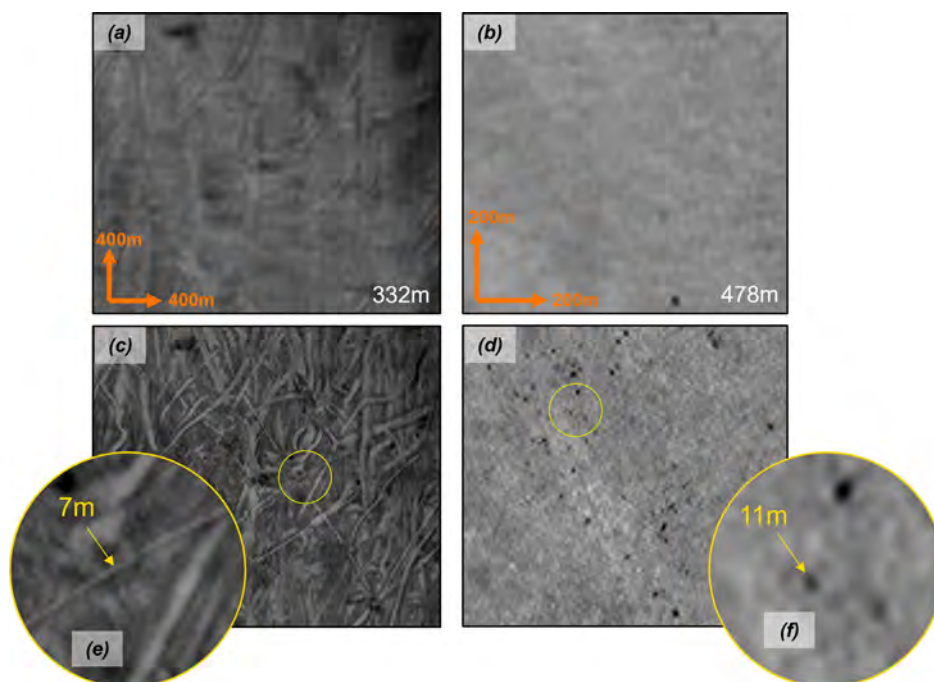
Figure 2 3D DAZ Q-Kirchhoff migration (a, b) compared to the 100 Hz TLFWI Image (c, d). Spatial resolution is significantly enhanced with FWI. Zoomed images reveal finer seabed details (e) and gas hazards (f) in the FWI Image as shown by Dinh et al., 2023.
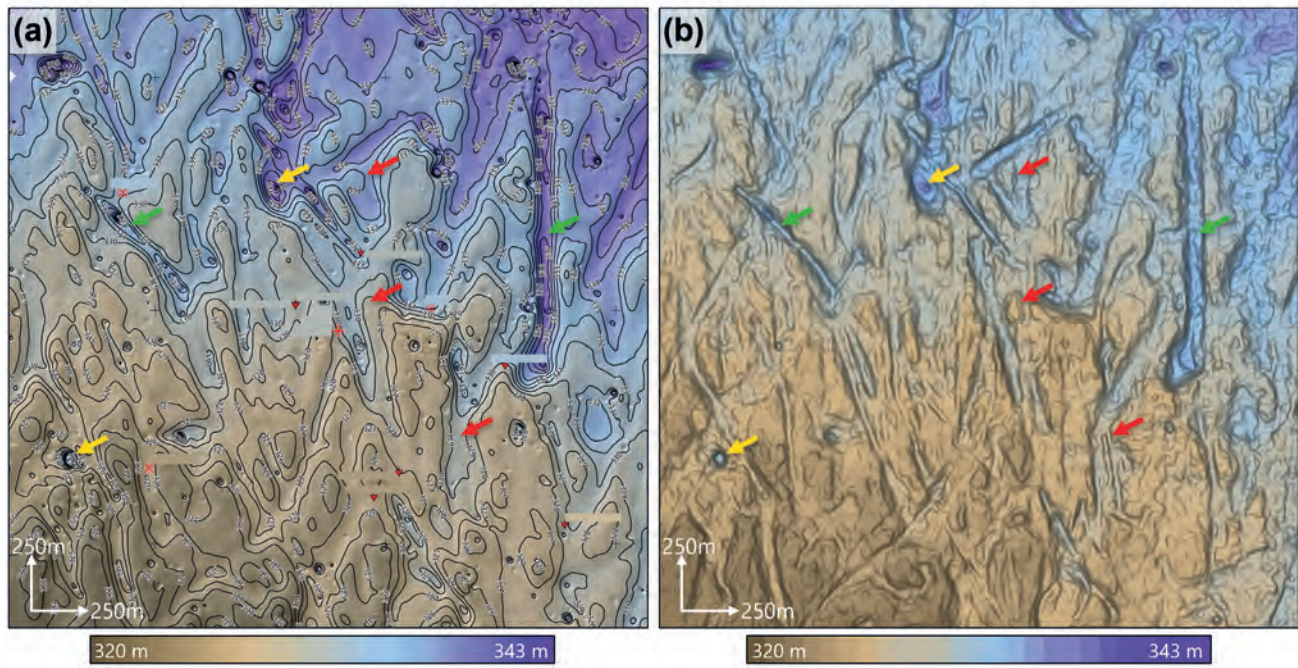
Figure 3 Site survey bathymetry map (a) shows the seabed with iceberg plough marks (green arrows) and pockmarks (yellow arrows). TLFWI maximum derivative map (b) shares similar features but adds spatial resolution (red arrows), as shown in Dinh et al. (2023).
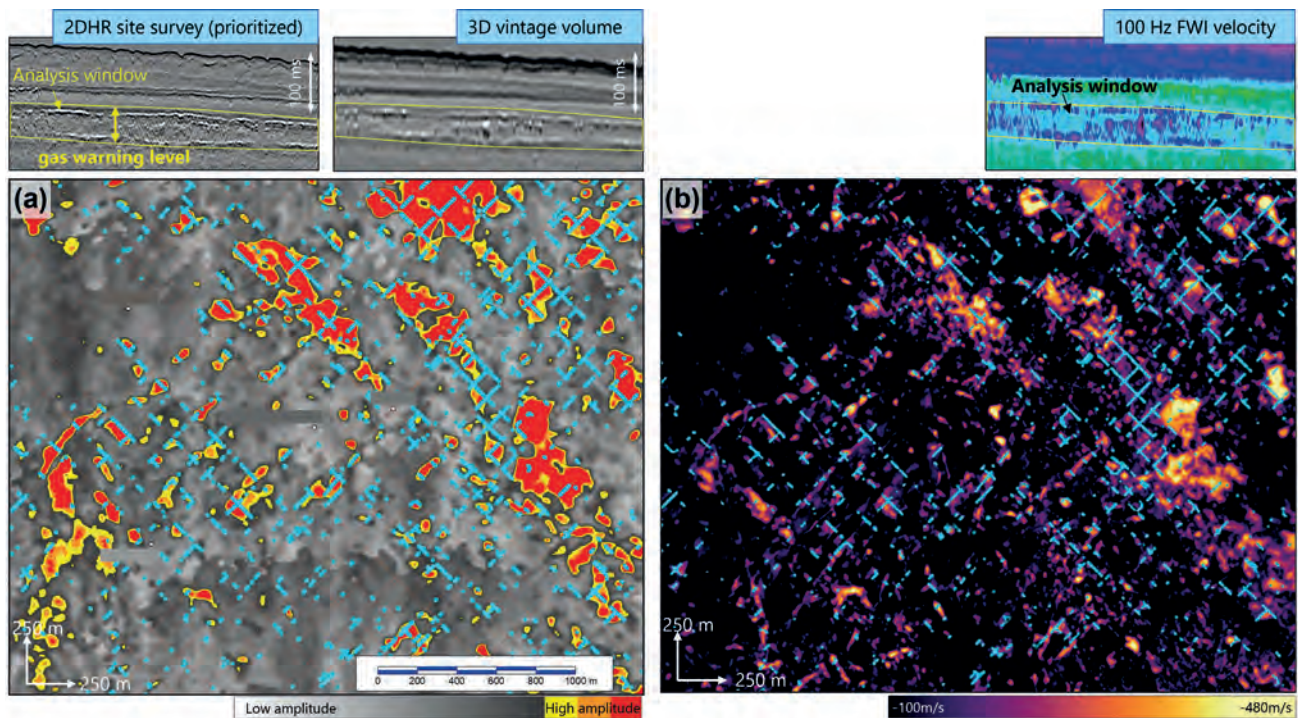
Figure 4 Site survey amplitude anomaly map (a), combining 2DHR amplitude anomalies and 3D Q-PSDM amplitude anomalies, shows a poor correlation. The corresponding FWI shallow gas amplitude map (b) shows better spatial resolution and resolves missing features.

FWI Imaging results

Figure 2 from Dinh et al. (2023) compares images from the 3D DAZ Q-Kirchhoff migration and 100 Hz TLFWI (calculated from Equation 1) using the same acquisition. Although it uses advanced DAZ processing techniques, the conventional imaging (Figure 2a, 2b) has lower lateral resolution compared to the FWI Image from the same acquisition (Figure 2c, 2d). The full-wavefield illumination and iterative least-squares data fitting process in FWI reveals fine features. For example, it shows buried iceberg scour marks and small-scale low impedance accumulations likely to be associated with gas (Figure 2e, 2f) that are less than 10 m wide, which are indistinguishable in the conventional imaging.

Site survey comparison
Bathymetry map

The bathymetry map derived from the MBES (Figure 3a) and the FWI-derived map (Equation 3, Figure 3b) show similar character-

istics, including multidirectional elongated iceberg plough marks (green arrows) and numerous depressed pockmarks (yellow arrows). Despite the high temporal resolution of the MBES, the FWI-derived map from the conventional 3D towed-streamer data provided significant uplift in lateral resolution, resolving small-scale features not detected by the site survey acquisition grid (red arrows).

Gas hazard map

The shallow gas map derived from the site survey data within the gas warning interval of 550-590 ms (Figure 4a) combines prioritised interpretations from 2DHR data (cyan colour) with 3D anomalies (red features) inferred from 3D Q-PSDM of conventional towed-streamer data. These show a low correlation, especially in the central area where numerous small-scale 2D anomalies are not confirmed by the 3D data. This mismatch may result from the limitations of 2D sampling, erroneous 2D imaging of out-of-plane subsurface reflectors, or the low spatial resolution of conventional 3D imaging. In contrast, FWI-derived anomalies extracted from within the corresponding depth interval (Equation 2, Figure 4b) show improved lateral resolution of features that could be inferred from the 3D data, enhancing geohazard interpretation potential.

Example 2

Data description

In this example, high-resolution FWI Imaging was applied in the Barents Sea, known for its rugged seafloor topography. In 2019, a seismic survey was conducted in water depths of 400 m, with a source-over-spread configuration using five 75 m-separated airgun arrays, positioned halfway along the 16 8 km-long, 62.5 m-spaced cables (top sources). The five sources were supplemented by an additional source array placed in front of the cables (front source) for longer offset coverage. This design provided dense spatial sampling and full-azimuth coverage at near offsets.

In 2023, a 2D high-resolution site survey was conducted over an area of prospective wells. Seismic data was acquired with a 400 Hz maximum source frequency, 96 channels, 1 ms

sample interval and 6.25 m CMP spacing. It also featured an ultra-high-resolution (UHR) data acquisition using a 1.6 kHz maximum source frequency, 32 channels, 0.25 ms data sampling, and a 1.5625 m bin size. A bathymetry map was derived from the site survey MBES measurements.

FWI Imaging was run up to 100 Hz on a 50 km^2 subset of the source-over-spread configured data, covering the 2D UHR site survey. From this dataset, a bathymetry map and geobody anomalies were extracted (Equations 2 and 3).

FWI Imaging results

The 100 Hz FWI image significantly improved the image quality compared to conventional Kirchhoff migration (Figure 5). The improved illumination and signal-to-noise ratio (SNR) allowed for the detection of multiple small-scale geobodies with clearer fault imaging. Shallow geology was better resolved, and evidence of fluid conduits was indicated by brighter amplitudes. Unlike the Kirchhoff migration, FWI Imaging did not struggle with structural imaging below shallow gas. This is likely due to the inherent illumination balancing and transmission loss compensating characteristics of the FWI algorithm.

Highlighting improvements in spatial resolution, Figures 6a and 6b show a coherence attribute comparison at 450 m depth. This was calculated from the Kirchhoff image and FWI Image (Equation 5) and is overlaid by the legacy velocity and FWI velocity model, respectively. This comparison demonstrates the significant uplift in detail of the FWI Image, featuring sharply defined, high-resolution overburden iceberg plough marks and small-scale velocity anomalies (sub-15 m wide). Figures 6c and 6d show this coherency comparison at 520 m depth, without the velocity overlays. At this depth, Figure 6e provides the addition of the FWI Image. The FWI Image coherency shows a complex network of regional faults, the most apparent of which is highlighted by the arrow in Figure 6d, and a highly illuminated local fractured zone, most visible in the FWI Image (Figure 6e). In contrast, the Kirchhoff image using the legacy velocity field did not detect fault activity at this depth due to lower SNR (Figure 6c).

Once these features were identified from corresponding attributes, they were converted and displayed as 3D geobodies to
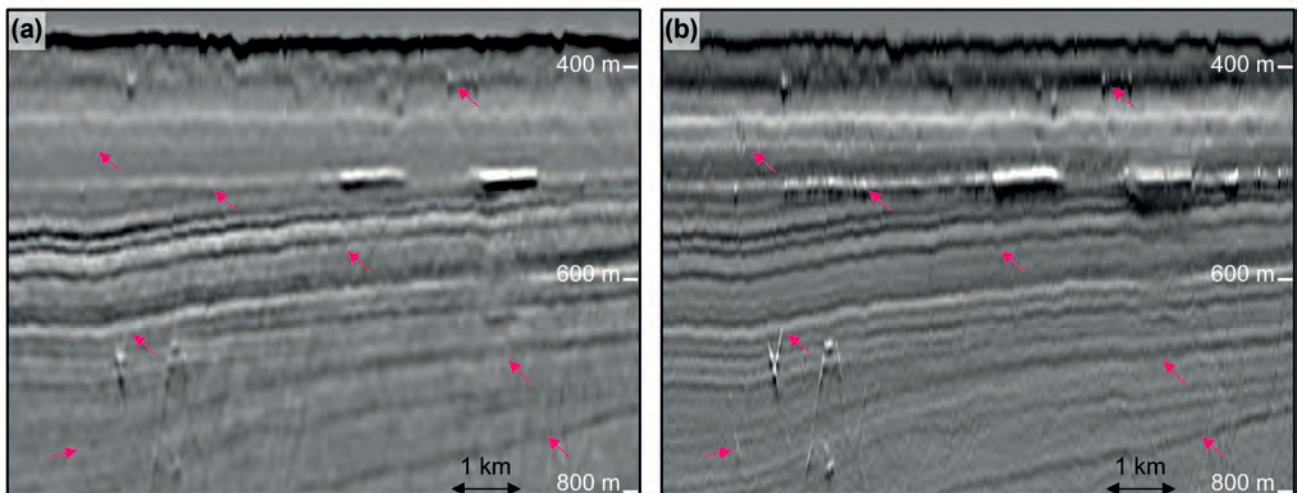
Figure 5 3D Q-Kirchhoff migration (a) compared to the FWI Image (b), both displayed to 100 Hz. Note improved SNR, illumination and structural imaging compared to the conventional image underneath the seabed and mid-section fault imaging.
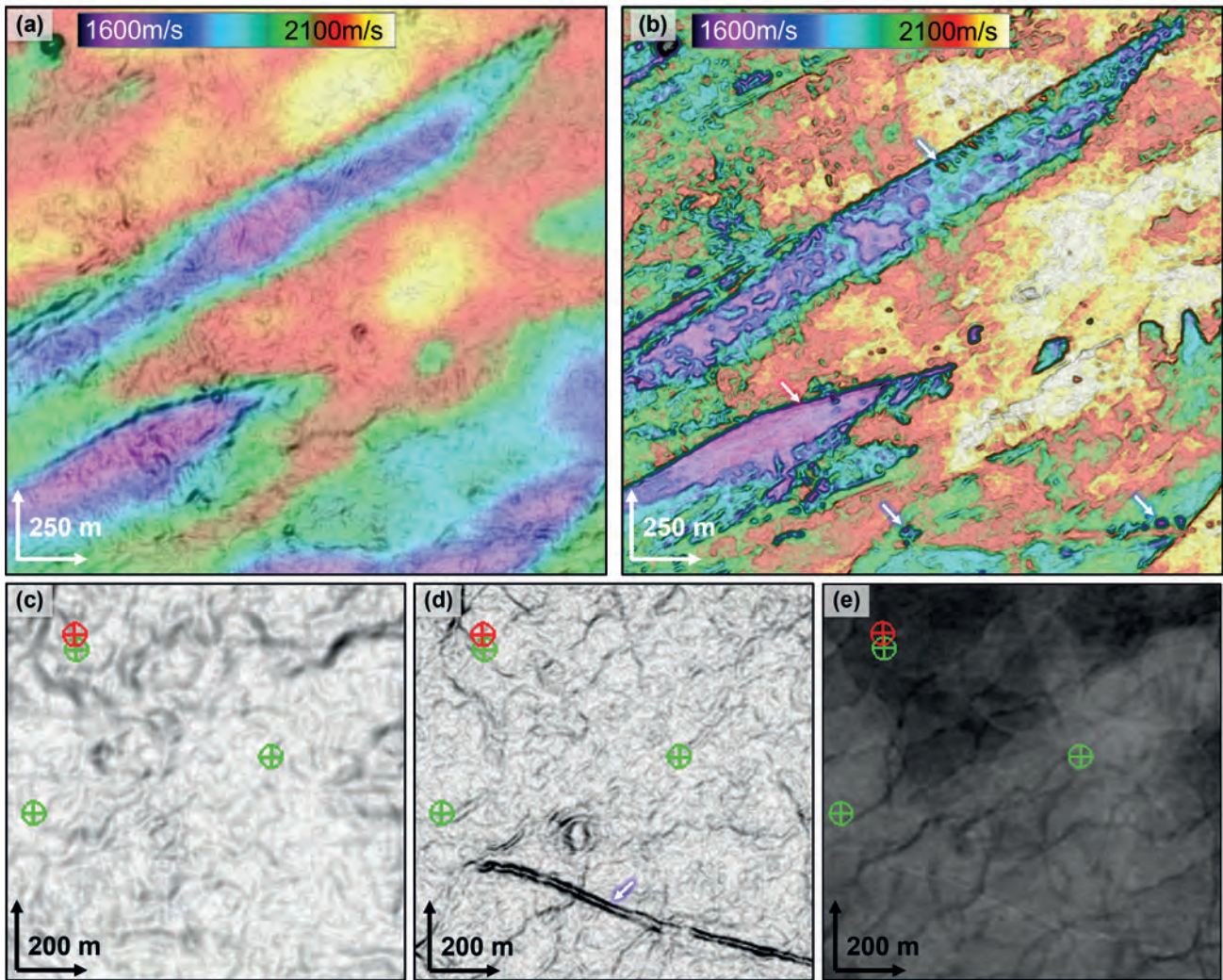
Figure 6 Coherence attribute and corresponding velocities at a 450 m depth from 3D Q-Kirchhoff migration (a) compared to the 100 Hz FWI Image (b) show uplift in spatial resolution in the FWI result, revealing a variety of potential hazards (white arrows). Example at 520 m shows fault imaging in the Q-PSDM coherency (c) has been improved in the FWI velocity coherency (d) and FWI Image (e). Crossed circles indicate well locations.
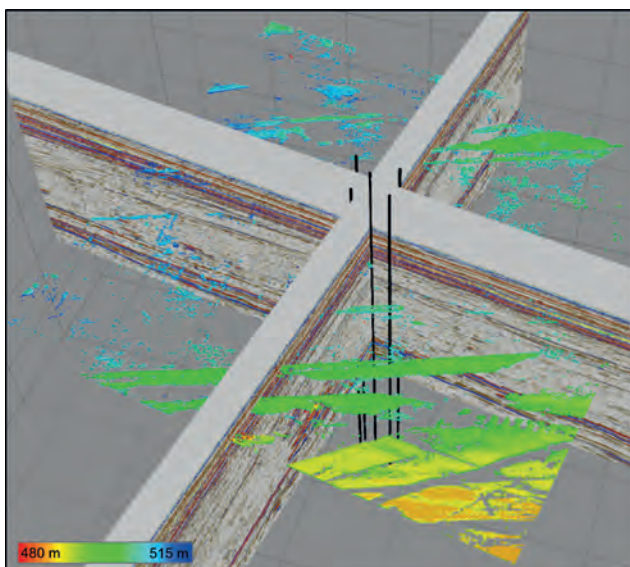
Figure 7 3D visualisation of low-amplitude anomalies as a tool for data integration and hazard analysis. Black lines indicate prospective well paths.

obtain a more comprehensive understanding of shallow hazards (Figure 7). Such visualisation can be integrated with information from other sources to reduce uncertainty and improve ground model accuracy.

Site survey comparison

The water bottom surface extracted from the FWI Image result exhibited a significant improvement in detail, resolving small-scale (sub-10 m wide) iceberg keels and pockmarks that were not detectable in the legacy Kirchhoff image (Figure 8). Compared with the site survey bathymetry map, all details were consistently captured in the FWI Image result. This observation demonstrated that high-frequency FWI Imaging for spatial resolution can provide comparable results to the MBES at the water bottom level, despite the data not being designed for this purpose.

Discussion

In both examples, the FWI-derived bathymetry map exhibited a high degree of correlation with the MBES-derived map. The hazard map, produced from conventional 3D data in the first exam-

ple, demonstrated the ability to enhance the spatial resolution and reduce uncertainty for shallow hazard identification compared to a benchmark site survey supplemented with conventional 3D imaging. The second example expanded the attribute technique to other potential hazards, such as boulders and fault systems, suggesting an effective visualisation tool to provide valuable insights into shallow geological features.

FWI will be influenced by the acquisition geometry. To validate the FWI Imaging in a coarser acquisition environment, the source-over-spread data from the second example was decimated to match a more conventional acquisition configuration (two 150 m-separated top sources with a 7.5 m actuation spacing every 30 m, and 62.5 m streamer separation with 12.5 m receiver spacing). A similar FWI workflow was then applied to this decimated data using the same starting model derived from a smoothed 13 Hz FWI velocity model. The results were then compared with the undecimated source-over-spread FWI results. Figure 9 is extracted from the centre of the test area. In the decimated data, we do notice some limitations in resolving steeply dipping events, limited illumination between sail lines, and some degradation in SNR (red arrows). Yet the 60 Hz FWI Images from both scenarios present comparable resolution at and beneath the seabed level, thanks to iterative data fitting and the full-wavefield sampling including primaries, ghosts, multiples, and diving waves. The use of high-order narrower-angle multiple ray paths helps to increase near-offset illumination. This is beneficial in shallow water areas where events may otherwise not be imaged owing to the post-critical refraction threshold. Combined with the first example, this observation has demonstrated that a conventional acquisition configuration can still be suitable for FWI Imaging,

and the technology still has potential even when dense data coverage is not always available.

In both examples, the crosstalk between velocity and other parameters, such as viscosity (attenuation) or density, has not been fully considered beyond a low-frequency update. Extending the FWI to either a multi-parameter visco-acoustic (described by Latter et al., 2023) or even visco-elastic workflow (Masmoudi et al., 2023) could reduce residual inversion error here. Once these crosstalk effects are properly accounted for, interpretable resolution is the next consideration. Regarding spatial resolution, the use of the full wavefield, including high-order multiples, can resolve finer details than conventional Kirchhoff migration at the same frequency, which relies on primary-only inputs. The FWI models show that the technology can resolve geobodies sub-10 m wide observed in both examples. Figures 10b and 10e also show that the FWI Image from conventional data has richer low frequencies compared to a dedicated site survey, in addition to the 3D sampling, recording aperture, and the lateral resolution accuracy improvements mentioned throughout this article. There are reasons, however, why high-frequency FWI Imaging from conventional towed-streamer 3D seismic may not replace dedicated HR site surveys. Site surveys offer superior vertical resolution and often provide supplementary information, including geotechnical data that conventional 3D data often does not provide. Also, site survey acquisition timing may be more favourable relative to infrastructure placement decisions as well as other potential insurance considerations. Nevertheless, the ability to leverage existing raw 3D exploration seismic data with minimal image processing to provide high-resolution data in a short timeframe is a significant advantage of the FWI Imaging
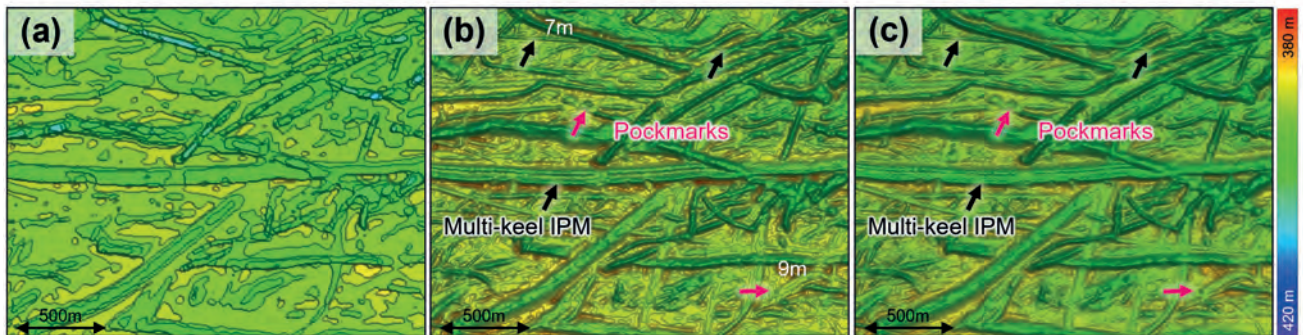
Figure 8 Seabed surface from Kirchhoff migration (a), 100 Hz FWI Image (b) and MBES site survey (c). Note that the FWI Image resolves consistent features to the dedicated MBES, such as multi-keel iceberg ploughmarks and pockmarks.
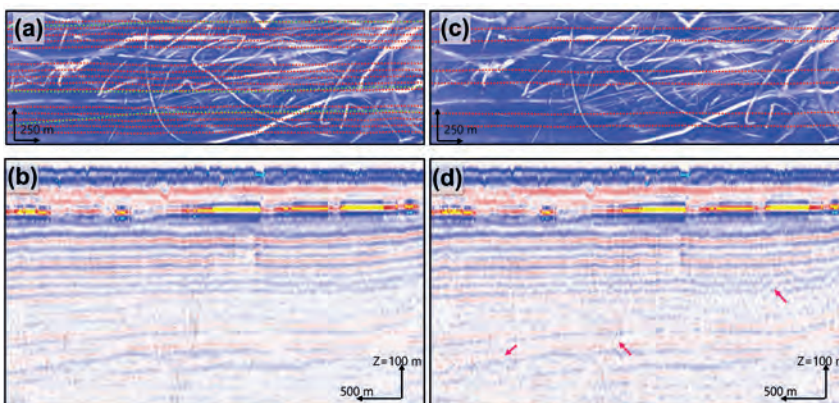
Figure 9 Comparison of the 60 Hz FWI results between full source-over-spread data (a and b) versus decimated source-over-spread data (c and d) in horizontal view (top row) and vertical view (bottom row). In the top view, red dots are top source shots and green dots are front source shots. In (c), only two top sources are used for FWI Imaging. The observations suggest the resilience of the technology to sparser data.
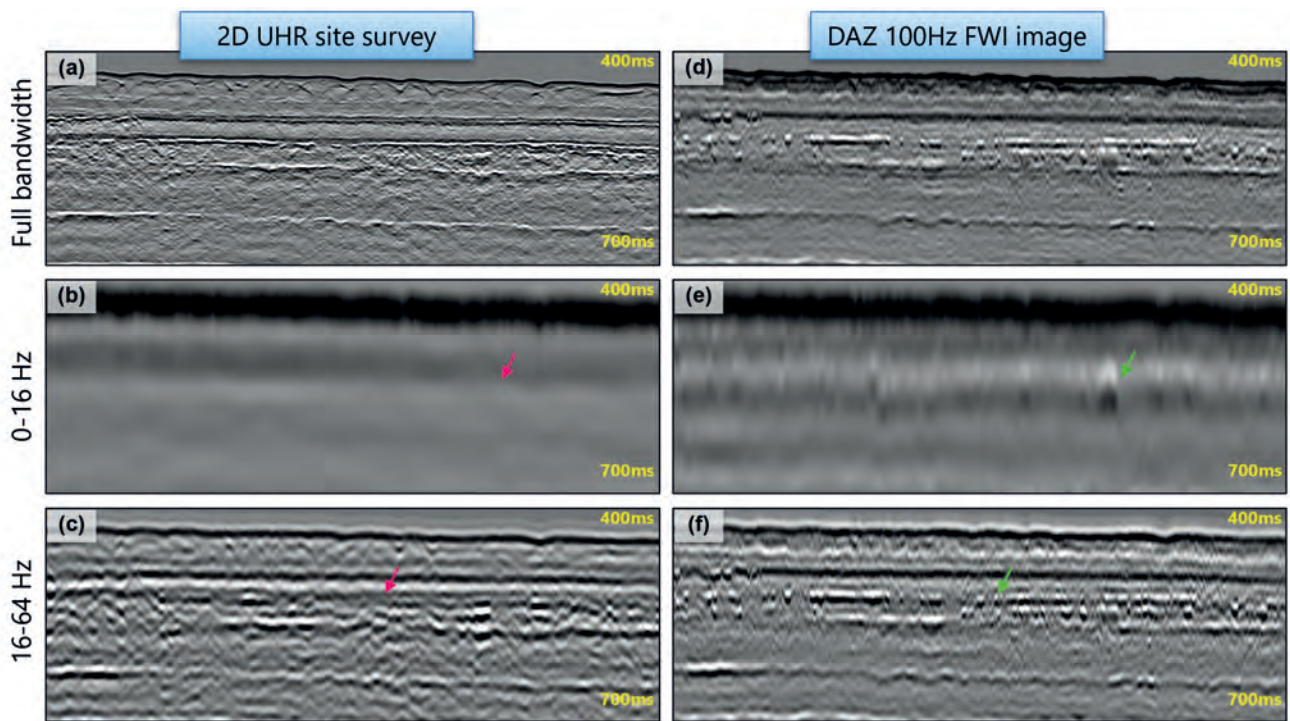
Figure 10 Bandwidth split indicates richer low-frequency content in the FWI Image (e and f) compared to the 2DUHR site survey (b and c) despite the limited upper bandwidth (d vs. a).

technology, bringing rapidly available supplementary information to guide or potentially reduce the scope of subsequent 2D or 3DHR site surveys.

Conclusions

We have presented an approach for shallow hazard analysis by repurposing conventional 3D towed-streamer seismic data as well as the application of high-frequency FWI Imaging techniques. Through additional attribute analysis on the FWI products, we have generated meaningful insights to identify potential anomalies, as demonstrated in two case studies which surpassed what could be achieved by conventional primary imaging approaches alone. High-frequency FWI Imaging can serve as a valuable complementary tool to dedicated HR data. The potential impact of this technology for shallow hazard analysis is significant. Where existing conventional 3D data is already present over the target area, it can provide cost-effective, rapid turnaround 3D results, to help directly identify risks or support better planning of dedicated surveys.

Acknowledgements

References

Bright, D., Jones, C.E., Belhassen, Y., Brasil, R., Macintyre, H. and França, C. [2015]. *Full Waveform Inversion for Shallow Hazard Identification on a Narrow Azimuth Dataset.* 77th EAGE Conference & Exhibition, WS10-C03.

Cooper, J. and Ratcliffe, A. [2023]. The role of FWI Imaging in compensating for transmission loss. *84th EAGE Conference & Exhibition, Extended Abstract.*

Dinh, H., Latter, T., Townsend, M. and Grinde N. [2023]. Dual-azimuth FWI Imaging and its potential in shallow hazard assessment. *84th EAGE Conference & Exhibition, Extended Abstract.*

Dinh, H., Beech, A., Hill, S., Latter, T., Høgden, S., Robb, N., Aksland, M. and Bertrand, M. [2024]. Source-over-spread high-resolution *FWI-based shallow hazard imaging in Barents Sea.* 2024 NPF Biennial Geophysical Seminar.

Douglas, G. [2011]. Site survey geophysical acquisition – a recent history and an idealized future. *FORCE geohazards seminar, Extended Abstract, 5.*

Espin, I., Salaun, N., Jiang, H. and Reinier, M. [2023]. From FWI to ultra-high-resolution imaging. *The Leading Edge,* **42**(1), 306-313.

Kanrar, A., Cooke, A., Lewis, O., Joyce, S., Keeble, J., Ghanem, A., Powis, D., Broadbent, K. and Francis, M. [2019]. High-Resolution Processing and Imaging for Shallow-Hazard Analysis: a Case Study from Angoche, Offshore Mozambique. *81st EAGE Conference & Exhibition, Extended Abstract.*

Kassarie, K., Mitchell, S., Albertin, M., Hill, A. and Carney, R. [2017]. Identifying and mitigating against potential seafloor and shallow drilling hazards at a complex Gulf of Mexico Deepwater site using HR3D seismic and AUV data. *Near Surface Geophysics,* **15**(4), 415-426.

Kerrison, H., Fallon, P., Kaszycka, E., Cichy, K., Ratcliffe, A. and Masmoudi, N. [2021]. Impact of streamer acquisition geometry on fwi imaging. *82nd EAGE Conference & Exhibition, Extended Abstract.*

Latter, T., Gram-Jensen, M., Buriola, F., Dinh, H., Faggetter, M., Jupp, R., Townsend, M., Grinde, N., Mathieu, C. and Byerley, G. [2022]. The value of dual-azimuth acquisition: imaging, inversion and development over the Dugong area. *83rd EAGE Conference & Exhibition, Extended Abstract.*

Latter, T., Nielsen, K-M., Beech, A. and Cantu Bendeck, D. [2023]. Deriving a high-resolution regional scale Q model over the Northern Viking Graben. *84th EAGE Conference & Exhibition, Extended Abstract*.

Li, R., Hongyan, L. and Denes, V. [2015]. The analysis of an FWI velocity model for potential shallow geohazard. *SEG Global Meeting Abstracts: Depth model building: Full-waveform inversion*, 62-64.

Lim, M., Huang, F., Haacke, R. and Davies, D. [2022]. Near-surface imaging in the Caspian Sea: Comparison of high-resolution towed-streamer, OBN multiple migration and NFH Imaging. *EAGE NSG2022 4th Conference on Geophysics for Mineral Exploration and Mining*, 1-5.

Lu, S. [2021]. Migration using sea surface-related multiples: Challenges and opportunities. *Geophysics*, **86**(5), WC11-WC19.

Masmoudi, N., Stone, W. and Ratcliffe, A. [2023]. Visco-elastic Full-waveform-inversion and Imaging using ocean-bottom node data. *84th EAGE Conference & Exhibition, Extended Abstract*.

Poole, G. [2021]. Least-squares multiple imaging constrained jointly by OBN and towed-streamer data, *82nd EAGE Conference & Exhibition, Extended Abstracts*.

Selvage, J., Jones, C. and Edgar, J. [2012]. Maximizing the value of 3D seismic data for shallow geohazard identification. *First Break,* **30**(8), 73-83.

Sharp, A. and Samuel, A. [2004]. An example study using conventional 3D seismic data to delineate shallow gas drilling hazards from the West Delta Deep Marine Concession, offshore Nile Delta, Egypt. *Petroleum Geoscience*, **10**(2), 121-129.

Sukmono, S., Machado, V., Adelina, R. and Ambarsari, D. [2017]. Integration of 3D seismic attributes for preliminary shallow geohazard identification in deep water exploration area with no well data. *First Break,* **35**(8), 91-97.

Tang, Q., Li, X., Mueller, A., Xie, Y., Hatnan, F., Wang, G., Hussaidon, F., Shorter, J. and Cannon, M. [2023]. Using least-squares wave-equation multiple migration for shallow imaging, a case study on offshore Brunei OBN data. *84th EAGE Conference & Exhibition, Extended Abstract*.

Tokarev, M., Pirogova, A., Roslyakov, A., Shalaeva, N., Terekhina, Y., Glubokovskikh, S. and Rybin, N. [2018]. Evaluation of Potential Geological Hazards in the Sea of Okhotsk from Conventional 3D Seismic Observations. *3rd Applied Shallow Marine Geophysics Conference, Extended Abstract*.

Tyagi, C., Leake, S., Mistry, K., Olsen, C. and Sundøy, K.J. [2021]. Utilizing near-field hydrophone data for high-resolution shallow hazard imaging. *82nd EAGE Conference & Exhibition, Extended Abstract*.

Vandrasi, V., Al-Waily, M., Mothi, S. and Vasquez, A. [2020]. Time-lag FWI based velocity model and image of a coarse shallow water OBC data set. *90th SEG Annual Meeting, Expanded Abstracts*, 715-719.

Wei, Z., Mei, J., Wu, Z., Zhang, Z., Huang, R. and Wang, P. [2023]. Pushing seismic resolution to the limit with FWI imaging. *The Leading Edge*, **42**(1), 24-32.

Wiarda, E.J., Shaw, S.A., Boiero, D., Gundersen, A. and West, L.R. [2014]. Integrating FWI with Surface-wave Inversion to Enhance Near-surface Modelling in a Shallow water Setting at Eldfisk. *76th EAGE Conference & Exhibition, Extended Abstract*.

Zhang, Z., Mei, J., Lin, F., Huang, R. and Wang, P. [2018]. Correcting for salt misinterpretation with full-waveform inversion. *88th SEG Annual International Meeting, Expanded Abstracts*, 1143-1147.

Zhang, Z., Wu, Z., Wei, Z., Mei, J., Huang, R. and Wang, P. [2020]. FWI Imaging: Full-wavefield imaging through full-waveform inversion. *90th SEG Annual Meeting, Expanded Abstracts*, 656-660.